Secondary Structures of Histone H3 Proteins with Unmethylated and Methylated Lysine-4 and -9 Residues: Characterization Using Circular Dichroism Spectroscopy

Yudai Izumi

Contents

Abstract Circular dichroism (CD) spectroscopy, especially that using synchrotron radiation as a light source, is a powerful tool for analyzing secondary structures of proteins in solution. In particular, CD spectroscopy allows observations of structural changes following post-translational modifications, such as methylation. In this chapter, techniques and measurement protocols are introduced. Recent structural analyses of H3 proteins before and after methylation of lysine-4 and -9 residues are also shown. In these CD spectroscopy analyses, mono- and dimethylation of H3 increased the presence of α-helical structures and decreased β-strand contents, whereas trimethylation decreased α-helix and increased β-strand contents. These structural alterations occurred at adjacent and distant residues from the methylated site.

Y. Izumi (✉)
Hiroshima Synchrotron Radiation Center, Hiroshima University, Higashi-Hiroshima, Hiroshima, Japan
e-mail: izumi-yudai@hiroshima-u.ac.jp

S. Jurga, J. Barciszewski (eds.), *The DNA, RNA, and Histone Methylomes*, RNA Technologies, https://doi.org/10.1007/978-3-030-14792-1_19

Keywords Epigenetics · Post-translational modification · Synchrotron radiation · Chiroptical spectroscopy · Lysine-specific demethylase 1 (LSD1/KDM1)

1 Introduction

Nucleosomes are octamers of four core histone proteins (H2A, H2B, H3, and H4) around which 146–147 base pairs of DNA are wrapped, and these are the building blocks of chromatin in eukaryotic nuclei (Luger et al. 1997; Davey et al. 2002). Post-translational modifications, such as methylation, of histones have been shown to play substantial roles in cellular functions. For example, methylation of H3 on lysine-4 (K4) and lysine-9 (K9) residues has been associated with transcriptionally active chromatin and inactive chromatin, respectively, in higher eukaryotes (Lachner and Jenuwein 2002). On the other hand, since the absence of K4-methylated H3 is required for DNA methylation, defects of which are linked to serious human diseases, such as cancer (Gal-Yam et al. 2008), demethylation of methylated H3 is also essential. Such methylation states are controlled by specific histone methyltransferases and demethylases.

Lysine-specific demethylase 1 (LSD1), also known as KDM1, was the first histone demethylase to be identified (Shi et al. 2004). LSD1 belongs to the flavin adenine dinucleotide dependent amine oxidase family (Shi et al. 2004; Shi 2007; Forneris et al. 2008) and converts K4 monomethylated or dimethylated H3 (H3K4me1 and H3K4me2, respectively) to unmethylated H3. On the other hand, it does not catalyze K4 trimethylated H3 (H3K4me3) (Shi et al. 2004). LSD1 has been associated with various important cellular processes (Zheng et al. 2015), but is reportedly overexpressed in several cancer cells (Ota and Suzuki 2018). Accordingly, LSD1 inhibitors are potential anti-cancer drugs (Suzuki and Miyata 2011; Maes et al. 2015; McAllister et al. 2016; Niwa and Umehara 2017). Indeed, some inhibitors have been tested in clinical trials for treatment of acute leukemia (Harris et al. 2012; Mohammad et al. 2015), small cell lung cancers (Mohammad et al. 2015), and neurodegenerative disorders (Niwa and Umehara 2017). In addition, novel LSD1 inhibitors are under development (Ogasawara et al. 2013; Maiques-Diaz and Somervaille 2016; Amano et al. 2017; Ota and Suzuki 2018).

Most LSD1 inhibitors, such as *trans*-2-phenylcyclopropylamine (Schmidt and McCafferty 2007) and above inhibitors, are complex unnatural molecules. However, histone H3 proteins are worthy of consideration as LSD1 inhibitors. Because the 21-mer peptides of H3 act as inhibitors of LSD1 (Forneris et al. 2005, 2006) and the binding affinity between full-length of unmethylated H3 and LSD1 is nearly 100-fold higher than that of the peptides (Burg et al. 2016). Hence, full-length unmethylated H3 may act as a good inhibitor. Since Forneris et al. also showed peptides of methylated, and mutated H3 (21-mer) acted as inhibitors of LSD1 (Forneris et al. 2005, 2006), other methylated H3 proteins may show similar activities.

Conformations of (un)methylated H3 have important functional implications for use as inhibitors of LSD1, because these are closely related to protein–protein

interactions (Tobi and Bahar 2005). However, unfortunately, yet no structural data for the full-length of non-nucleosomal H3 are available in the Protein Data Bank, although structural data for nucleosomes (Luger et al. 1997; Davey et al. 2002) and (un)methylated H3 peptides in complexes with various histone-binding proteins, including LSD1 (Yang et al. 2007), can be found.

Recently, our group analyzed secondary structures of full-length K4- or K9-methylated H3 using circular dichroism (CD) spectroscopy and compared these with unmethylated H3. These primary investigations of full-length (un)methylated H3 conformations showed that methylation at K4 or K9 induces structural changes in H3 at residues both adjacent and distant from methylated sites (Izumi et al. 2018a, b). In this chapter, these results are introduced to facilitate further studies of the interactions between full-length (un)methylated H3 and LSD1 and other histone binding proteins. Next section, experimental methods for analyzing protein structures using CD spectroscopy is introduced. In Sect. 3, the experimental results are shown. In the last section, brief summary is described.

2 CD Spectroscopy

Standard CD spectroscopy procedures for analyses of protein structures are reviewed thoroughly elsewhere (for example, Greenfield 2006; Miles and Wallace 2006). Thus, in this section, these techniques and measurement protocols are introduced, only briefly.

2.1 Circularly Polarized Light

Light is an electromagnetic wave. When the electric field of the light oscillates randomly in time, the light is called unpolarized light. Most light sources, such as sunlight, incandescent bulbs, and Xe lamps, emit unpolarized light. If the unpolarized light passes through appropriate prisms and filters, such as Pockels cells, the electric field oscillates sinusoidally in a single plane (Fig. 1a), and then the light is classified as linearly polarized light. When the electric field of the light consists of two perpendicular electromagnetic plane waves, which are equal in amplitude, but have a phase difference of 90° (quarter of the wavelength), the tip of the electric field vector rotates in a circle around the direction of propagation (Fig. 1b). Such polarized light is called circularly polarized light (CPL). More comprehensible animated graphics of the CPL can be found on the internet. CPL is often converted from linearly polarized light using quarter wave plates in laboratories. CPL is classified into two types depending on the rotation direction. Viewing from the receiver, if the vector of the CPL rotates clockwise, the CPL is called as right circularly polarized light (RCPL). In the opposite case, that is, the vector rotates counterclockwise, it is called as left circularly polarized light (LCPL).

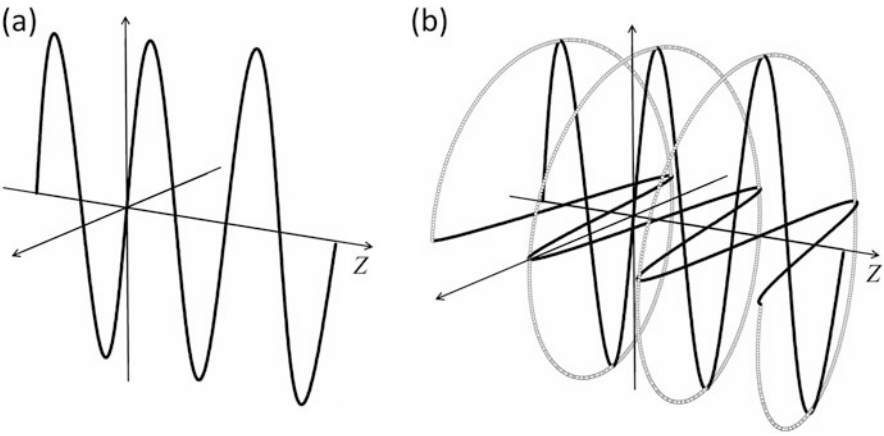

Fig. 1 The electric fields of (**a**) linearly polarized light and (**b**) RCPL propagating along *Z*-axis

2.2 CD and Its Notations

CD is a phenomenon exhibited in absorption bands of optical active molecules, such as amino acids, riboses, and deoxyriboses, and defined as the difference between the molar absorption coefficient for LCPL (ε_L) and that for RCPL (ε_R) as in the following equation: $\Delta\varepsilon = \varepsilon_L - \varepsilon_R$ (in M^{-1} cm^{-1}). As a consequence, CD spectroscopy is a variation of absorption spectroscopy. The CD value $\Delta\varepsilon$ is sometimes referred to as molar CD. However, for historical reasons, different notation, ellipticity, is also used to express the CD intensities. Indeed, commercial CD spectrophotometers often return CD spectra in terms of ellipticity.

Ellipticity θ' (in rad) is derived from the ratio of electric vector magnitudes of LCPL and RCPL (E_L and E_R, respectively):

$$\tan\theta' = \frac{E_R - E_L}{E_R + E_L} \tag{1}$$

Molar CD and ellipticity are interconverted as follows. Using Beer-Lambert's law, the Eq. (1) is rewritten as

$$\tan\theta' = \frac{\exp\left(\frac{\ln 10}{2}\Delta\varepsilon\, C\, l\right) - 1}{\exp\left(\frac{\ln 10}{2}\Delta\varepsilon\, C\, l\right) + 1} \tag{2}$$

where C and l are the concentration of the sample (in M) and the path length of the cuvette (in cm). Since, in general, θ' and $\Delta\varepsilon$ are small, the above equation can be approximated to be

$$\theta' = \frac{\ln 10}{4}\Delta\varepsilon\, C\, l \tag{3}$$

In accord with tradition, converting the unit of ellipticity from radians to millidegrees and calculating the constant term, we can obtain

$$\Delta\varepsilon = \frac{\theta}{32980\ C\ l} \tag{4}$$

where θ is ellipticity (in millidegrees). Thus, the ellipticity provided as the data from CD spectrophotometers can be converted to molar CD using the Eq. (4). It is noted that, in the case of CD spectroscopy of proteins, mean residue molar concentration, namely molar concentration multiplied by number of amino acid residues in the protein, is used as C. Instead of molar CD, mean residues molar ellipticity [θ] (in degrees $cm^2\ dmol^{-1}$) is also commonly used to describe CD intensities and is calculated as follows: $[\theta] = 3298\ \Delta\varepsilon$.

2.3 *Advantages of CD Spectroscopy Using Synchrotron Radiation*

CD spectroscopy can be performed using commercial CD spectrophotometers. However, the author would like to recommend the usage of synchrotron radiation (SR) CD beamlines (Miles and Wallace 2006). Since the photon flux from the Xe lamps, that are used as light sources for commercial CD spectrophotometers, severely decreases in the vacuum ultraviolet (VUV) region (wavelength < ~200 nm), it is hard to obtain meaningful data below ~190 nm. Alternatively, since photon flux of SR is higher than that for Xe lamps in the VUV region, the use of SR can extend CD spectra to the wavelength region below 190 nm and thereby can provide additional information which is unobtainable using commercial CD instruments. In particular, the use of SR is essential for CD measurements of chiral molecules which compose only from single bonds, such as saccharides, since CD peaks of assigned to $n \rightarrow \sigma^*$ and $\sigma \rightarrow \sigma^*$ transitions are detectable only below 190 nm (Arndt and Stevens 1993).

At the time of writing, SR-CD beamlines were available for use at the following eight SR facilities to my knowledge (Table 1): Hiroshima Synchrotron Radiation Center (HiSOR) of Hiroshima University in Japan (Matsuo and Gekko 2013), Institute for Storage Ring Facilities (ISA) of Aarhus University in Denmark (Miles et al. 2007), Beijing Synchrotron Radiation Facility (BSRF) in China (Tao et al. 2009), National Synchrotron Radiation Research Center (NSRRC) in Taiwan (Liu et al. 2010), Diamond Light Source (DLS) in UK (Hussain et al. 2012), Synchrotron SOLEIL in France (Réfrégiers et al. 2012), BESSY-II of the Helmholtz-Zentrum Berlin (Reichardt et al. 2001), and ANKA of Karlsruhe Institute of Technology (Bürck et al. 2015) in Germany. In general, these beamlines can be used after acceptance of proposal(s), which can be referred to websites of each SR facility (Table 1).

Table 1 The list of the SR facilities equipped with SR-CD beamlines[a]

Location	SR facility	URL
Japan	HiSOR	http://www.hsrc.hiroshima-u.ac.jp/english/index.html
Denmark	ISA	http://www.isa.au.dk/index.asp
China	BSRF	http://english.bsrf.ihep.cas.cn/
Taiwan	NSRRC	http://www.nsrrc.org.tw/
UK	DLS	https://www.diamond.ac.uk/Home.html
France	SOLEIL	https://www.synchrotron-soleil.fr/en
Germany	BESSY-II	https://www.helmholtz-berlin.de/quellen/bessy/index_en.html
Germany	ANKA	https://www.anka.kit.edu/

[a]At the time of writing

2.4 Structural Analyses of Proteins Using CD Spectroscopy

Structural information of proteins from CD spectra is limited compared with that from X-ray crystallography and nuclear magnetic resonance (NMR), both of which display three-dimensional structures with atomic-level resolutions. CD spectroscopy is, nonetheless, a powerful tool because it provides structural information, including structural dynamics, with greater ease than that using above techniques. In particular, (1) required sample quantities are only 1–10% of those required for X-ray crystallography and NMR (Kim et al. 2008) and (2) the samples can be prepared by simply dissolving the protein in a solvent. In addition, neither crystallization nor isotopic substitution is required, and sample losses and accidental denaturation during sample preparation are negligible in most cases.

Each protein forms individual conformation, but includes common structures called as secondary structures, for example, α-helices and β-strands, which compose β-sheets connecting laterally, turns and unordered structures, also known as random coil or disordered structures. Therefore, it is assumed that CD spectra of a protein are linear combinations of CD spectra from each of these secondary structures weighted by relative abundance, as indicated in the following equation (Greenfield 2006):

$$\mathrm{CD}(\lambda) = \sum_s f_s \Delta\varepsilon_s(\lambda) \tag{5}$$

where CD(λ) is the CD intensity of an unknown protein at wavelength λ, f_s is the fraction of the secondary structure s (s = α-helix, β-strand, . . .), and $\Delta\varepsilon_s(\lambda)$ is the CD intensity of secondary structure s at wavelength λ. Given a protein comprising some α-helices, β-strands, turns, and unordered structures at fractions of 25% ($f_s = 0.25$), CD spectra of the protein can be described as follows:

$$\mathrm{CD}(\lambda) = 0.25\left(\Delta\varepsilon_{\alpha\text{-helix}}(\lambda) + \Delta\varepsilon_{\beta\text{-strand}}(\lambda) + \Delta\varepsilon_{\mathrm{turn}}(\lambda) + \Delta\varepsilon_{\mathrm{Unordered}}(\lambda)\right) \tag{6}$$

Thus, if $\Delta\varepsilon_s(\lambda)$ is known, we can estimate secondary structure contents of unknown proteins f_s by deconvoluting the CD spectrum. Values of $\Delta\varepsilon_s(\lambda)$ are

often derived empirically from reference datasets of CD spectra for numerous proteins whose structures have been determined by X-ray crystallography. These secondary structures have characteristic CD peaks (for example, Matsuo et al. 2005) that are predominantly assigned to $n \rightarrow \pi^*$ and $\pi \rightarrow \pi^*$ transitions of peptide bonds in the UV–VUV region (Woody 1995). α-Helices exhibit a positive peak around 190 nm and two negative peaks at around 208 and 222 nm, and another positive peak appears as a shoulder around 175 nm. β-Strands are characterized by a negative peak and a positive peak at 218 and 195 nm, respectively, and unordered structures give negative peaks at around 200 nm and two positive peaks around 170 and 225 nm.

Whereas analytical procedures for CD spectroscopy may appear complex, various programs have been developed for analyzing CD spectra and these are publicly available (For example, Sreerama and Woody 2000; Whitmore and Wallace 2004; Micsonai et al. 2015). The analyses using these programs are easily performed only inputting CD data of proteins you measured and the calculations are completed in a short time using standard personal computers or the internet.

2.5 Experimental Procedure for CD Spectroscopy

2.5.1 Sample Preparation

CD spectra of proteins are usually measured in liquid solutions, which can be prepared easily by simply dissolving the protein in a solvent, as mentioned above. However, solvents should be carefully selected, especially for VUV-CD measurements (Miles and Wallace 2006). Chloride ions exhibit strong absorption bands in the VUV region and can hence interfere with VUV-CD measurements by severely decreasing the transmitted light intensity, even when using SR. Therefore, sodium chloride, which is often supplemented in protein solutions, had better be substituted with sodium fluoride or removed if possible. Similarly, Tris buffer should be acidified with phosphoric acid instead of HCl. Although phosphate buffers are preferable, concentrations should be kept as low as possible.

The path length of the sample-cells used in VUV-CD measurements is often below ~100 μm to reduce absorption of solvents, and it is shorter than that used in conventional CD measurements (1–10 mm). Observed CD intensities, such as ellipticity θ, are proportional to the sample concentration and the path length of the sample-cell. According to Beer-Lambert's law, when the path length decreases by 1/10, ten-fold sample concentrations are required to observe the same ellipticity. Thus, to obtain meaningful CD signals, concentrations of samples used in VUV-CD measurements need to be much higher than those used in conventional CD measurements. In general, optimal concentrations of proteins for use with a path length of 10 μm are 10 mg/mL for α-helical proteins and 15–20 mg/mL for β-sheet rich proteins (Miles and Wallace 2006).

2.5.2 Sample-Cell

Although various types of sample-cells are commercially available, custom-made sample-cells are often used at SR-CD beamlines (for example, Wien and Wallace 2005; Izumi and Matsuo 2018). Because short path length cells are preferable, demountable cells that are easier to clean are often used. In addition, sample cells for VUV-CD spectroscopy are often made of CaF_2 glasses (Wien and Wallace 2005) because transmittance of these in the VUV region is higher than that of the SiO_2 glasses used in conventional CD spectroscopy (cut-off wavelength, ~140 nm for CaF_2 vs. ~160 nm for SiO_2).

As an example, a sample cell recently developed is described (Izumi and Matsuo 2018). It is comprised of two circular glasses. One of the glasses has a counterbore hole and the other is flat, and the depth of the counterbore hole corresponds with the path length of the cell. After placing sample solution into the counterbore hole on the first glass, it is covered with another glass and the glasses are then fixed in the sample-cell holder and used for CD spectroscopy. Sample volumes are generally 2–3 μL to avoid foaming, although convenient volumes depend on the types of solutions and skills of users.

2.5.3 Measurements and Analyses of CD Spectra

The CD measurement systems used in SR-CD beamlines are similar to those of commercial CD spectrophotometers, although important details should be referred to in the publications and websites of each beamline (Reichardt et al. 2001; Miles et al. 2007; Tao et al. 2009; Liu et al. 2010; Hussain et al. 2012; Réfrégiers et al. 2012; Matsuo and Gekko 2013; Bürck et al. 2015). In general, SR emitted from a storage ring, which is linearly polarized light, is monochromated and converted to LCPL or RCPL using a phase shifter (photo-elastic modulator) (Fig. 2). Intensities of transmitted LCPL and RCPL passing through the sample are detected using a detector (photomultiplier tube) (Fig. 2) and CD spectra are then generated.

Before analyzing CD spectra, measured CD intensities, ellipticity θ, must be converted to molar CD (Δε) or mean residue molar ellipticity [θ] values, because magnitudes of θ depend on the concentration of the sample and the path length of the

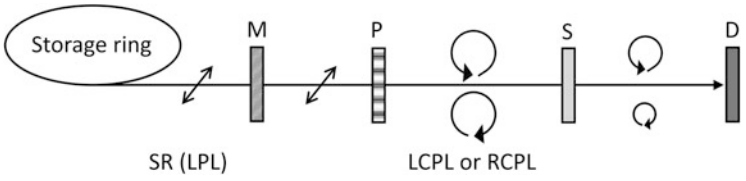

Fig. 2 A schematic view of SR-CD beamlines. *SR* synchrotron radiation, *LPL* linearly polarized light, *M* monochromator, *P* phase shifter (photo-elastic modulator), *L(R)CPL* left (right) circularly polarized light, *S* sample, *D* detector (photomultiplier tube)

cuvette as shown in Sect. 2.2. Spectra can then be analyzed using empirical programs, as mentioned above (For example, Sreerama and Woody 2000; Whitmore and Wallace 2004; Micsonai et al. 2015).

3 Secondary Structures of K4- or K9-(Un)methylated H3

3.1 CD Spectra of K4- or K9-(Un)methylated H3

Figure 3 shows the CD spectra of unmethylated H3, H3K4me1, H3K4me2, and H3K4me3 in 25-mM sodium phosphate buffer supplemented with 250-mM sodium fluoride. The CD spectrum for unmethylated H3 exhibited a positive peak at ~190 nm and two negative peaks at ~210 and ~220 nm. These peaks are characteristic of α-helix structures. H3K4me1 and H3K4me2 had similar CD spectra. It might be a reasonable result because both H3K4me1 and H3K4me2 are substrates of LSD1 (Shi et al. 2004), although these proteins are nucleosomal in cells. Positive peaks of H3K4me1 and H3K4me2 shifted toward the longer-wavelength region, whereas negative peaks shifted toward the shorter-wavelength region compared with those of unmethylated H3. CD peak intensities of H3K4me1 and H3K4me2 were higher than those of unmethylated H3. In contrast, negative CD peaks of H3K4me3 shifted further toward the shorter-wavelength region and their intensities were increased compared with those of H3K4me1 and H3K4me2. Although the positions of the positive peaks around 190 nm were similar for all three H3K4 methylation states, the intensities of those in H3K4me3 were decreased compared with H3K4me1 and H3K4me2 peaks.

Figure 4 shows the CD spectra of mono-, di-, and trimethylated H3 at residue K9 (H3K9me1, H3K9me2, and H3K9me3, respectively) in the same solvent. The CD spectrum of unmethylated H3 is also shown again for comparison. CD spectral shapes of H3K9me1 and H3K9me2 were similar, although the widths of positive peaks differed. Positive CD peak positions of H3K9me1 and H3K9me2 shifted toward the longer-wavelength region, and their intensities were the highest among

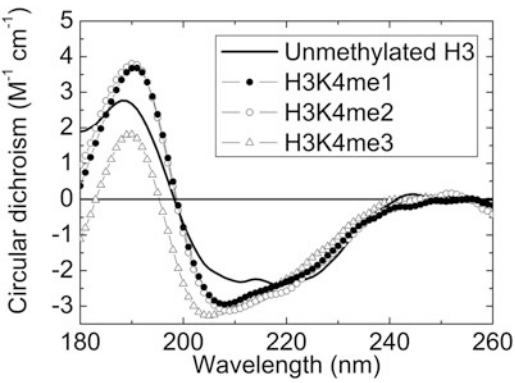

Fig. 3 CD spectra of unmethylated H3 (solid line), H3K4me1 (closed circle), H3K4me2 (open circle), and H3K4me3 (open triangle)

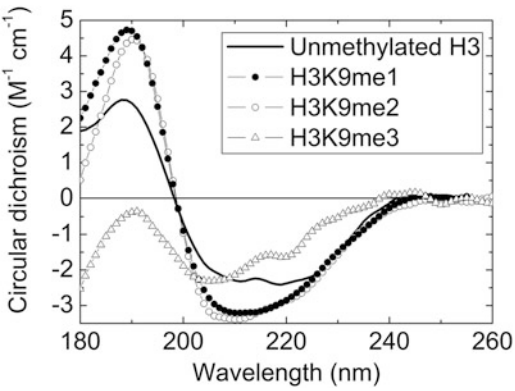

Fig. 4 CD spectra of unmethylated H3 (solid line), H3K9me1 (closed circle), H3K9me2 (open circle), and H3K9me3 (open triangle)

the samples examined. Negative peak intensities of methylated H3K9 were also higher than those of unmethylated H3. Finally, H3K9me3 showed negative peaks at ~200–220 nm but no positive peak at ~190 nm, and the spectral shape differed substantially from those of other samples.

In comparisons of the CD spectra of K4- and K9-methylated H3 and unmethylated H3 (Figs. 3 and 4), spectral shapes depended on the positions and degrees of methylation. Because CD spectra reflect secondary structures of proteins, these results show that (1) methylation of K4 and K9 residues induces structural alterations of H3 and (2) that these methylated H3 form different structures from each other.

3.2 Secondary Structure Contents of K4- or K9-(Un) methylated H3

Analyses of CD spectra were performed using the SELCON3 program (Sreerama et al. 1999; Sreerama and Woody 2000) with the reference dataset that was generated at HiSOR (Matsuo et al. 2004, 2005). The secondary structure contents of K4- or K9-(un)methylated H3 and their standard deviations are listed in Table 2, in which secondary structure contents are normalized to a total amount of 100%. Numbers of segments in secondary structures are also listed in Table 2. For ease of comparison, the results in Table 2 are shown in the proportional histograms of the secondary structure contents seen in Fig. 5. The contents of monomethylated H3 were within a standard deviation of those of dimethylated H3, and these are shown together in Table 2 and Fig. 5. H3K4me1 and H3K4me2 showed incremental differences in secondary structure contents and segment numbers of α-helix structures, compared with those of unmethylated H3. In contrast, the contents and numbers of β-strand structures were less in H3K4me1 and H3K4me2 than in unmethylated H3. Further methylation (trimethylation of K4 in H3; H3K4me3) decreased α-helix contents and incrementally increased β-strand contents, compared with those of H3K4me1 and H3K4me2. Decreased unordered structures were observed in H3K4me1 and

Table 2 Secondary structure contents of (un)methylated H3

Structure content (%)	H3	H3K4me1 H3K4me2	H3K4me3	H3K9me1 H3K9me2	H3K9me3
α-Helix	25.0 ± 1.2	30.7 ± 1.3	21.8 ± 0.8	36.5 ± 1.7	13.1 ± 0.8
β-Strand	21.3 ± 1.5	18.9 ± 2.0	25.1 ± 2.0	13.6 ± 2.6	29.6 ± 1.9
Turn	21.1 ± 1.0	23.5 ± 1.2	21.4 ± 0.7	23.1 ± 1.0	22.7 ± 1.2
Unordered	32.7 ± 1.7	27.0 ± 1.8	31.7 ± 1.6	27.8 ± 1.8	36.3 ± 2.4
Numbers of α-Helices	4	5	4	6	3
Numbers of β-Strands	6	5	7	4	8

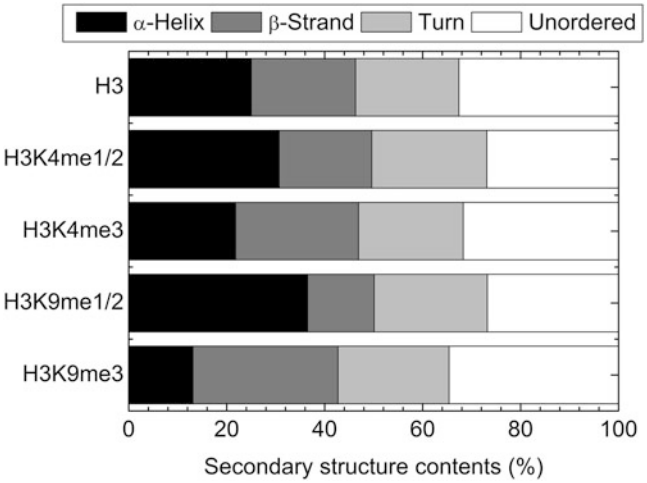

Fig. 5 Comparison of secondary structure contents of (un)methylated H3 normalized to a total content of 100%

H3K4me2 compared with those in unmethylated H3, whereas those structures were almost equally prevalent in H3K4me3 and unmethylated H3.

The tendency of K9 methylation to induce structural alterations was similar to that of K4 methylation, except that more drastic structural changes were induced by the former. H3K9me1 (H3K9me2) showed the highest contents and numbers of α-helix structures and the smallest contents and segment numbers of β-strand structures. Conversely, contents and segment numbers of β-strand structures were greatest in H3K9me3, in which α-helix contents were the smallest.

3.3 Predicted Positions of α-Helices and β-Strands

Based on CD spectroscopy results, the positions of α-helices and β-strands in (un) methylated H3 were predicted using a neural network (NN) method, which is termed

the VUVCD-NN combination method. This original method was developed at HiSOR, and the computational protocol is described elsewhere (Matsuo et al. 2008). Briefly, an NN algorithm was used to predict the positions of secondary structures using evolutionary sequence information based on the position-specific scoring matrices generated by the PSI-BLAST algorithm (Jones 1999). These computations were performed with reference to the numbers of α-helix and β-strand segments and the numbers of amino acid residues forming α-helix and β-strand structures, as determined in CD spectroscopy and SELCON3 analyses. The accuracy of the VUVCD-NN combination method is reportedly about 75% for 30 reference proteins (Matsuo et al. 2008).

Figure 6 shows predicted secondary structure sequences of samples. Turn and unordered structures were estimated using SELCON3 analysis and were classified as "others". In analyses of unmethylated H3, structures from the 1st to the 44th residues were assigned as others (turn or unordered structures), and were consistent with the crystal structure of nucleosomal H3 (Davey et al. 2002). In contrast, simulations of methylated H3 showed the formation of a β-strand structure from 5th to 8th residues. In H3K9me3, another β-strand structure was assigned at the 39th–42th residues. It was also predicted that structural alterations would not be limited to methylated regions. For example, α-helix formations were predicted at the 65th to 69th, 80th to 83rd, and 85th to 86th residues in H3K4me1 and H3K4me2, although these α-helices reverted to other structures in H3K4me3. Similar structural changes, such as increased α-helices with monomethylation and demethylation and decreased α-helices with trimethylation, were predicted for K9 methylation. However, the amount of structural changes induced by K4 methylation was less than those following K9 methylation.

In comparisons with predicted structures, the structure of H3K4me3 was almost the same as that of unmethylated H3, except for the β-strand at the N-terminal tail. Therefore, the full-length of H3K4me3 may act as an inhibitor of LSD1 with similar potency as that of full-length unmethylated H3. In agreement, the 21-mer peptide of H3K4me3 was characterized as an inhibitor of LSD1 previously (Forneris et al. 2006). However, the structures of K9-trimethylated H3 differed from those of K4-trimethylated and unmethylated H3, and therefore full-length K9-trimethylated H3 may have different effects on LSD1 or other proteins comparing to K4-trimethylated and unmethylated H3.

Although the causes of these differences have not yet been unidentified, structural alterations of H3 that depend on degrees and positions of methylation may be of interest for application as drugs. Future studies will examine binding affinities between full-length methylated H3 and various enzymes, including LSD1.

3.4 Structural Alterations Following K4 or K9 Methylation in Solution

The VUVCD-NN combination method predicted that K4 and K9 methylation induces structural changes of H3 at adjacent and distal residues from the methylated sites. These data suggest that structural alterations are induced by interactions

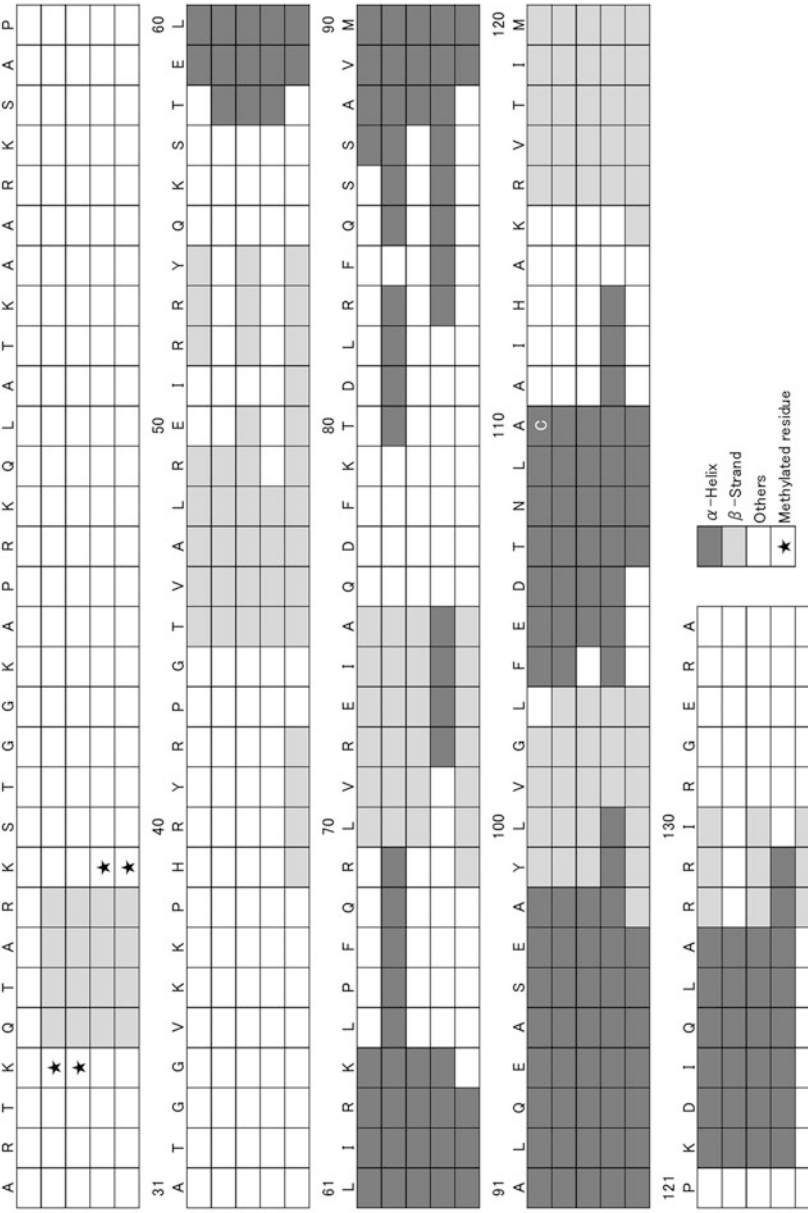

Fig. 6 Sequence-based secondary structures of (un)methylated H3 as predicted using the VUVCD-NN method; α-helix, β-strand, and other structures are shown in dark gray, gray, and white rectangles, respectively. The star in the rectangle shows the methylated residue. The 110th residue of unmethylated H3 is cysteine (C) and differs from that of methylated H3 (alanine; A)

between residues that are distant from the methylation site, such as residues 65th to 86th in H3K4me1, and the methylated N-terminal tail. In the unmodified state, the N-terminal tail may not interact with other domains, as observed in nucleosomal H3 (Davey et al. 2002). Conversely, K4 or K9 mono- or dimethylation alters steric barriers and/or electrostatic interactions around the methylation site, and these likely drive the formation of secondary structures at the N-terminal tail. These methylation related structural changes could also promote interactions between the N-terminal tail and residues that are distant from the methylation site, leading to the formation of α-helix structure(s). Structural changes following trimethylation may be similar, except that the distant residues form β-strand and other structures through these interactions. Similar structural changes were previously observed following phosphorylation of OdHI (Barthe et al. 2009). Specifically, phosphorylation induced folding of the unordered region so that the phosphorylated residue bound to its own FHA domain, and an α-helix was formed at distal residues.

To describe mechanisms that lead to the structural changes induced by K4 or K9 methylation, more precise theoretical simulations, such as molecular dynamics simulations, are important and will be interesting subjects of future work.

4 Summary

SR-CD spectroscopy revealed that methylation of H3 at K4 or K9 residues induces structural alterations and the data suggest that these alterations occur in adjacent and distal residues from the methylated site. CD data also indicate that H3K4me3 forms a similar structure to that of unmethylated H3, which acts as an inhibitor of LSD1. Because these conformations are closely related to protein–protein interactions, H3K4me3 may also act as an inhibitor of LSD1. Future studies are warranted to investigate binding affinities between H3K4me3 and LSD1. Cyclopedic CD spectroscopy of other methylated histones will also form the basis of future studies into the properties of methylated histones as inhibitors of LSD1.

Acknowledgments CD spectroscopy was performed with the approval of the Hiroshima Synchrotron Radiation Center of Hiroshima University (proposal numbers: 15A48, 16AU007, and 16BG018). The author is grateful to Drs. Kentaro Fujii and Akinori Yokoya (National Institutes for Quantum and Radiological Science and Technology, QST), Profs. Koichi Matsuo, Hirofumi Namatame, and Masaki Taniguchi (Hiroshima University) for their kind support. This work was supported by JSPS KAKENHI grant numbers JP15K16130 and JP17K12825.

References

Amano Y, Umezawa N, Sato S et al (2017) Activation of lysine-specific demethylase 1 inhibitor peptide by redox-controlled cleavage of a traceless linker. Bioorg Med Chem 25:1227–1234

Arndt ER, Stevens ES (1993) Vacuum ultraviolet circular dichroism studies of simple saccharides. J Am Chem Soc 115:7849–7853

Barthe P, Roumestand C, Canova MJ et al (2009) Dynamic and structural characterization of bacterial FHA protein reveals a new autoinhibition mechanism. Structure 17:568–578
Bürck J, Roth S, Windisch D et al (2015) UV-CD12: synchrotron radiation circular dichroism beamline at ANKA. J Synchrotron Radiat 22:844–852
Burg JM, Gonzalez JJ, Maksimchuk KR et al (2016) Lysine-specific demethylase 1A (KDM1A/LSD1): product recognition and kinetic analysis of full-length histones. Biochemist 55:1652–1662
Davey CA, Sargent DF, Luger K et al (2002) Solvent mediated interactions in the structure of the nucleosome core particle at 1.9 Å resolution. J Mol Biol 319:1097–1113
Forneris F, Binda C, Vanoni MA et al (2005) Human histone demethylase LSD1 reads the histone code. J Biol Chem 280:41360–41365
Forneris F, Binda C, Dall'Aglio A et al (2006) A highly specific mechanism of histone H3-K4 recognition by histone demethylase LSD1. J Biol Chem 281:35289–35295
Forneris F, Binda C, Battaglioli E et al (2008) LSD1: oxidative chemistry for multifaceted functions in chromatin regulation. Trends Biochem Sci 33:181–189
Gal-Yam EN, Saito Y, Egger G et al (2008) Cancer epigenetics: modifications, screening, and therapy. Annu Rev Med 59:267–280
Greenfield N (2006) Using circular dichroism spectra to estimate protein secondary structure. Nat Protoc 1:2876–2890
Harris WJ, Huang X, Lynch JT et al (2012) The histone demethylase KDM1A sustains the oncogenic potemtial of MLL-AF9 leukemia stem cells. Cancer Cell 21:473–487
Hussain R, Jávorfi T, Siligardi G (2012) Circular dichroism beamline B23 at the Diamond Light Source. J Synchrotron Radiat 19:132–135
Izumi Y, Matsuo K (2018) Sample-volume reduction using the Schwarzschild objective for a circular dichroism spectrophotometer and an application to the structural analysis of lysine-36 trimethylated histone H3 protein. Molecules 23:2865(1)–2865(12)
Izumi Y, Matsuo K, Fujii K et al (2018a) Circular dichroism spectroscopic study on structural alterations of histones induced by post-translational modifications in DNA damage responses: lysine-9 methylation of H3. J Radiat Res 59:108–115
Izumi Y, Matsuo K, Namatame H (2018b) Structural analysis of lysine-4 methylated histone H3 proteins using synchrotron radiation circular dichroism spectroscopy. Chirality 30:536–540
Jones DT (1999) Protein secondary structure prediction based on position-specific scoring matrices. J Mol Biol 292:195–202
Kim Y, Bigelow L, Borovilos M et al (2008) High-throughput protein purification for X-ray crystallography and NMR. Adv Protein Chem Struct Biol 75:85–105
Lachner M, Jenuwein T (2002) The many faces of histone lysine methylation. Curr Opin Cell Biol 14:286–298
Liu S-H, Lin Y-H, Huang L-J et al (2010) Design and construction of a compact end-station at NSRRC for circular-dichroism spectra in the vacuum-ultraviolet region. J Synchrotron Radiat 17:761–768
Luger K, Mäder AW, Richmond RK et al (1997) Crystal structure of the nucleosome core particle at 2.8 Å resolution. Nature 389:251–260
Maes T, Carceller E, Salas J et al (2015) Advances in the development of histone lysine demethylase innibitors. Curr Opin Pharmacol 23:52–60
Maiques-Diaz A, Somervaille TC (2016) LSD1: biologic roles and therapeutic targeting. Epigenomics 8:1103–1116
Matsuo K, Gekko K (2013) Construction of a synchrotron-radiation vacuum-ultraviolet circular-dichroism spectrophotometer and its application to the structural analysis of biomolecules. Bull Chem Soc Jpn 86:675–689
Matsuo K, Yonehara R, Gekko K (2004) Secondary-structure analysis of proteins by vacuum-ultraviolet circular dichroism spectroscopy. J Biochem 135:405–411
Matsuo K, Yonehara R, Gekko K (2005) Improved estimation of the secondary structures of proteins by vacuum-ultraviolet circular dichroism spectroscopy. J Biochem 138:79–88

Matsuo K, Watanabe H, Gekko K (2008) Improved sequence-based prediction of protein secondary structures by combining vacuum-ultraviolet circular dichroism spectroscopy with neural network. Proteins 73:104–112
McAllister TE, England KS, Hopkinson RJ et al (2016) Recent progress in histone demethylase inhibitors. J Med Chem 59:1308–1329
Micsonai A, Wien F, Kernya L et al (2015) Accurate secondary structure prediction and fold recognition for circular dichroism spectroscopy. Proc Natl Acad Sci USA 112:E3095–E3103. http://bestsel.elte.hu/index.php
Miles AJ, Wallace BA (2006) Synchrotron radiation circular dichroism spectroscopy of proteins and applications in structural and functional genomics. Chem Soc Rev 35:39–51
Miles AJ, Hoffmann SV, Tao Y et al (2007) Synchrotron radiation circular dichroism (SRCD) spectroscopy: new beamlines and new applications in biology. Spectroscopy 21:245–255
Mohammad HP, Smitheman KN, Kamat CD et al (2015) A DNA hypomethylation signature predicts antitumor activity of LSD1 inhibitors in SCLC. Cancer Cell 28:57–69
Niwa H, Umehara T (2017) Structural insight into inhibitors of flavin adenine dinucleotide-dependent lysine demethylases. Epigenetics 12:340–352
Ogasawara D, Itoh Y, Tsumoto H et al (2013) Lysine-specific demethylase 1-selective inactivators: Protein-targeted drug delivery mechanism. Angew Chem Int Ed 52:8620–8624
Ota Y, Suzuki T (2018) Drug design concepts for LSD1-selective inhibitors. Chem Rec 18:1–11
Réfrégiers M, Wien F, Ta H-P et al (2012) DISCO synchrotron-radiation circular-dichroism endstation at SOLEIL. J Synchrotron Radiat 19:831–835
Reichardt G, Bahrdt J, Schmidt J-S et al (2001) A 10 m-normal incidence monochromator at the quasi-periodic undulator U125-2 at BESSY II. Nucl Inst Methods Phys Res A 467-468:462–465
Schmidt DMZ, McCafferty DG (2007) *trans*-2-Phenylcyclopropylamine is a mechanism-based inactivator of the histone demethylase LSD1. Biochemist 45:4408–4416
Shi Y (2007) Histone lysine demethylases: emerging roles in development, physiology and disease. Nat Rev Genet 8:829–833
Shi Y, Lan F, Matson C et al (2004) Histone demethylation mediated by the nuclear amine oxidase homolog LSD1. Cell 119:941–953
Sreerama N, Woody RW (2000) Estimation of protein secondary structure from circular dichroism spectra: comparison of CONTIN, SELCON, and CDSSTR methods with an expanded reference set. Anal Biochem 287:252–260. https://sites.bmb.colostate.edu/sreeram/CDPro/
Sreerama N, Venyaminov SY, Woody RW (1999) Estimation of the number of α-helical and β-strand segments in proteins using circular dichroism spectroscopy. Protein Sci 8:370–380
Suzuki T, Miyata N (2011) Lysine demethylases inhibitors. J Med Chem 54:8236–8250
Tao Y, Huang Y, Gao Z et al (2009) Developing VUV spectroscopy for protein folding and material luminescence on beamline 4B8 at the Beijing Synchrotron Radiation Facility. J Synchrotron Radiat 16:857–863
Tobi D, Bahar I (2005) Structural changes involved in protein binding correlate with intrinsic motions of proteins in the unbound state. Proc Natl Acad Sci USA 102:18908–18913
Whitmore L, Wallace BA (2004) DICHROWEB, an online server for protein secondary structure analyses from circular dichroism spectroscopic data. Nucleic Acids Res 32:W688–W673. http://dichroweb.cryst.bbk.ac.uk/html/home.shtml
Wien F, Wallace BA (2005) Calcium fluoride micro cells for synchrotron radiation circular dichroism spectroscopy. Appl Spectrosc 59:1109–1113
Woody RW (1995) Circular dichroism. Methods Enzymol 246:34–71
Yang M, Culhane JC, Szewzuk LM et al (2007) Structural basis of histone demethylation by LSD1 revealed by suicide inactivation. Nat Struct Mol Biol 14:535–539
Zheng Y-C, Ma J, Wang Z et al (2015) A systematic review of histone lysine-specific demethylase 1 and its inhibitors. Med Res Rev 35:1032–1071